JGR Atmospheres

RESEARCH ARTICLE
10.1029/2020JD032894

Impact of Convectively Detrained Ice Crystals on the Humidity of the Tropical Tropopause Layer in Boreal Winter

R. Ueyama[1], E. J. Jensen[2], L. Pfister[1], M. Krämer[3,4], A. Afchine[3], and M. Schoeberl[5]

[1]NASA Ames Research Center, Moffett Field, CA, USA, [2]NCAR, Boulder, CO, USA, [3]Institute for Energy and Climate Research-Stratosphere (IEK-7), Forschungzentrum Jülich, Jülich, Germany, [4]Institute for Physics of the Atmosphere, Johannes Gutenberg University, Mainz, Germany, [5]Science and Technology Corporation, Columbia, MD, USA

Abstract Deep convection detraining in the uppermost tropical troposphere is capable of transporting water vapor and ice into the tropical tropopause layer (TTL), but the impact of deep convection on the global and regional TTL water vapor budget remains uncertain. In particular, the role of convectively detrained ice crystals that remain suspended after active convection has subsided is not well understood. These ice crystals represent aging cirrus anvils detached from the convective core. We use a cloud microphysical model that tracks individual ice crystals throughout their lifetimes to quantify the impact of detrained ice on the humidity of the TTL during boreal winter. Convective influence of air parcels near the wintertime cold point tropical tropopause is determined by tracing thousands of backward trajectories through satellite-derived, global, 3-hourly convective cloud-top altitude fields. Detrained ice, most of which is found over the tropical western Pacific, experiences cooling on the order of 1 K day^{-1} downstream of convection. Downstream cooling increases relative humidity and explains the observed supersaturated TTL over this region. Vapor in excess of saturation condenses onto the detrained ice, which ultimately brings the relative humidity down to saturation. Thus, convectively detrained ice crystals in aging anvils predominantly dehydrate the TTL, but the effect is small (0.01 ppmv). Moistening by active convection (0.30 ppmv), including the rapid sublimation of convectively lofted ice crystals near the tops of core anvils, overwhelms the dehydration by aging anvil ice crystals detrained from the core. The net effect is moistening by convective core anvils during boreal winter.

Plain Language Summary Tall towering clouds in the tropics are capable of transporting water vapor and ice crystals upward to an otherwise dry region of the atmosphere. Some ice crystals remain suspended in the upper atmosphere long after the cloud tower has collapsed, but their impact on the humidity of the upper atmosphere is unknown. We use a computer model to simulate the life cycle of these ice crystals to show that they generally dry the tropical atmosphere at 14–19 km during boreal winter by a small amount. This is because most of the ice crystals from tall towering clouds originate over the tropical western Pacific where they experience cooling, causing them to grow by extracting moisture from the surrounding atmosphere. Moistening of the environment by the cloud tower itself is much larger than the drying effect of suspended ice crystals in boreal winter. Even a small change in the humidity of the upper atmosphere above ~17 km significantly affects Earth's climate. Therefore, it is important to understand the processes that affect the humidity of tropical air at these altitudes, including temperature changes downstream of tall towering clouds that determine the fate of ice crystals ejected from these clouds.

Key Points:
- Convectively detrained ice crystals that remain after active convection has subsided are tracked individually in a cloud model
- Convectively detrained ice crystals in aging anvils over the western Pacific dehydrate near the wintertime cold point tropopause
- Growth and sublimation of ice crystals in aging anvils have a relatively minor impact on water vapor in the tropical tropopause layer

Correspondence to:
R. Ueyama,
rei.ueyama@nasa.gov

Citation:
Ueyama, R., Jensen, E. J., Pfister, L., Krämer, M., Afchine, A., & Schoeberl, M. (2020). Impact of convectively detrained ice crystals on the humidity of the tropical tropopause layer in boreal winter. *Journal of Geophysical Research: Atmospheres*, *125*, e2020JD032894. https://doi.org/10.1029/2020JD032894

Received 7 APR 2020
Accepted 3 JUL 2020
Accepted article online 7 JUL 2020

Author Contributions:
Conceptualization: R. Ueyama
Formal analysis: R. Ueyama
Funding acquisition: R. Ueyama
Methodology: R. Ueyama, E. J. Jensen
Supervision: E. J. Jensen
Writing - original draft: R. Ueyama
Writing – review & editing: R. Ueyama, E. J. Jensen

1. Introduction

The tropical troposphere is characterized by strong deep convection over the continents and the western Pacific Ocean that transports and redistributes energy, water vapor, and other trace constituents throughout the atmosphere up to the convective outflow altitude of about 12–14 km (Folkins & Martin, 2005). Even stronger convection, while less frequent, can at times reach the tropical tropopause level ~17 km or beyond (Danielsen, 1993; Zipser et al., 2006), raising the possibility of its impact on the composition of the tropical tropopause layer (TTL) (Fueglistaler et al., 2009) and the stratosphere (Corti et al., 2008; Danielsen, 1982; Kritz et al., 1993). This study focuses on the impact of deep convection on the humidity of the TTL near the wintertime cold point tropopause.

There has been considerable debate regarding the extent to which strong deep convection extending into the TTL may affect stratospheric humidity. To first order, stratospheric water vapor is controlled by the freeze drying of air transiting through the cold tropical tropopause in the tropical upwelling branch of the large-scale stratospheric Brewer-Dobson circulation (Brewer, 1949). However, various modeling studies have shown that small-scale processes such as waves, cloud microphysics and radiative heating, and convection all regulate TTL humidity to varying degrees (Bonazzola & Haynes, 2004; Dinh & Fueglistaler, 2014; Jensen & Pfister, 2004; Liu et al., 2010; Schoeberl et al., 2014, 2016, 2018; Schoeberl & Dessler, 2011; Ueyama et al., 2015, 2018). Although these processes are of secondary importance compared to the tropical tropopause temperature, their relative contributions vary regionally and seasonally. In particular, convection in the uppermost troposphere can significantly modulate the humidity of the TTL and possibly of the stratosphere as well, if convection reaches or overshoots the cold point tropopause. Even small amounts of water vapor in the stratosphere can significantly impact the radiative energy budget (Forster & Shine, 2002; Riese et al., 2012; Solomon et al., 2010) and stratospheric ozone chemistry (Dvortsov & Solomon, 2001; Stenke & Grewe, 2005; Vogel et al., 2011), and thus, understanding the detailed processes and accurately simulating them in chemistry-climate models is of key importance. Comprehensive modeling of the TTL has so far proven to be challenging.

Analysis of the convective impact is complicated by the fact that convection can either hydrate or dehydrate the TTL under different scenarios. On the one hand, deep convection cools the cold point tropopause, which can enhance dehydration (Kim et al., 2018; Kuang & Bretherton, 2004; Robinson & Sherwood, 2006). On the other hand, deep convection can moisten the TTL by directly transporting water vapor and ice, even across the tropopause in some cases (Chaboureau et al., 2007; Corti et al., 2008; Danielsen, 1993; Dessler et al., 2007; Grosvenor et al., 2007; Krämer et al., 2020; Nielsen et al., 2007; Schiller et al., 2009; Sherwood & Dessler, 2001; Smith et al., 2017). Global trajectory analyses with convective influence have demonstrated that convection generally hydrates the TTL and the lower stratosphere (Schoeberl et al., 2014, 2018, 2019; Ueyama et al., 2015, 2018), but the relative contributions of convective hydration and the large-scale circulation to the regional water vapor budget in different seasons are still poorly constrained.

A key element of the convective process that is often ignored or misrepresented in models is the convectively detrained ice crystals. Convection saturates the air within the convective plume by transporting relatively moist boundary layer air upward and by the adiabatic cooling of lofted air. Additionally, convective updrafts transport ice crystals to the convective cloud-top altitude. Observations of ice crystals above the tropical cold point tropopause (Corti et al., 2008; Krämer et al., 2020; Nielsen et al., 2007; Schiller et al., 2009) and the observed enrichment of water vapor isotopes in the TTL and lower stratosphere (Johnson et al., 2001; Keith, 2000; Moyer et al., 1996; Randel et al., 2012) are consistent with detrainment of ice from overshooting convection. A model study by Jensen et al. (2007) showed that the impact of detrained ice is determined by the relative humidity with respect to ice in the TTL: If the TTL is initially subsaturated, ice crystals lofted from deep convection will sublimate and rehydrate the air, whereas deep convection into supersaturated TTL air will dehydrate, as vapor in excess of saturation condenses on the ice crystals. Accordingly, some of the convectively detrained ice crystals in the TTL will sublimate or grow to establish or maintain saturation (i.e., ice saturation ratio of unity) in the anvil.

Entrainment of subsaturated or supersaturated environmental air is rampant at the tops of fresh deep convection, which presumably drives significant sublimation or deposition growth of detrained ice crystals within the active convective plume and fresh anvil. Active convection generally collapses within a few hours, but cirrus anvils can persist much longer (Mace et al., 2006; Pfister et al., 2001), leaving behind detrained ice crystals that can be transported away from the original convective event. Thus, in essence, the total impact of deep convection on TTL humidity can be separated into two parts: (i) near-instantaneous *convective saturation* (which may include the rapid growth or sublimation of lofted ice crystals within the plume and fresh anvil) and (ii) the delayed impact of *detrained ice crystals* in aging anvils detached from the convective core. The first effect is commonly referred to as "convective moistening" as deep convection into the TTL often entrains subsaturated air which causes ice crystals to sublimate and moisten the TTL in convective core anvils. However, we prefer to use the term "convective saturation" in order to include convective dehydration events in supersaturated TTL air. The focus of this study is on the second effect: aging anvil ice crystals detrained from the convective core. In situ measurements have provided evidence of detrained ice crystals

some distance from the original convection (Nielsen et al., 2007), but our knowledge of their impact on TTL humidity is limited. This is because quantifying their impact requires a consideration of the variability on a wide range of scales encountered by the detrained ice crystals throughout their lifetimes. These processes include, but not limited to, submesoscale cloud motions driven by cloud radiative heating, mesoscale dynamics associated with the convection, and synoptic-scale systems that affect the evolution of the ice cloud downstream of the convection.

Some studies have argued that convectively lofted ice crystals can significantly moisten the lower stratosphere (Avery et al., 2017; Dessler et al., 2007, 2016; Wang et al., 2019; Ye et al., 2018), while other studies have found negligible impact of these ice crystals on the TTL and stratospheric humidity (Schoeberl et al., 2018; Ueyama et al., 2018). We will show that the detrained ice impact on TTL humidity during boreal winter is negligible or rather a very slight dehydration. We argue that the apparent discrepancy between our study's results and those of other studies that find significant moistening by detrained ice is primarily because of the different definitions of the detrained ice effect. With the exception of some recent work (Schoeberl et al., 2018; Ueyama et al., 2015, 2018), most other studies (e.g., Dessler et al., 2007; Ye et al., 2018) define the detrained ice effect to include the rapid moistening by deep convection, which may include the sublimation of lofted ice crystals within the (subsaturated) convective core anvil. These studies neglect the impact of detrained ice crystals that remain after active convection has subsided.

The goal of this study is to quantify the impact of convectively detrained ice crystals that persist after active convection has subsided (hereafter referred to as "detrained ice") on the global and regional humidity in the TTL. We consider ice crystals that are detrained from deep convection penetrating the TTL, some of which may overshoot the cold point tropical tropopause. The detrained ice simulated in this study represents aging cirrus anvils that are detached from the convective core. We use a cloud microphysical model that tracks individual ice crystals throughout their lifetimes and calculates their effect on the TTL humidity. Mesoscale dynamics driven by the convection and cloud-scale motions driven by cloud radiative heating are not included in our simulations but could be important as they impact temperatures in the vicinity of convective systems. We also assume that all convective influence events occur with relatively old clouds that remain after entrainment near the tops of fresh convection has largely subsided (i.e., about a few hours). This is a reasonable assumption since the time scale of convective formation of the cirrus anvil is much shorter than the time scale of the decay of the anvil which is on the order of 6 to 12 hr based on cirrus cloud observations at the islands of Manus and Nauru in the western and central equatorial Pacific (Mace et al., 2006). We discuss the implications of these assumptions on this study's results in section 4.

The paper is structured as follows: Section 2 describes the data sets used and methodology employed. Section 3 presents the results of one-dimensional cloud microphysical model driven by time-height curtains of ERA-Interim temperatures along thousands of parcel trajectories launched backward from the tropics near the tropical mean cold point tropopause level. Convective influence is determined by tracing the trajectories through satellite-derived convective cloud-top altitude fields. Sensitivities of the detrained ice impact on TTL humidity to ice size distribution and ice water content are examined in an idealized model; these results are also discussed in section 3. Section 4 summarizes the results of this study and discusses them in the context of previous works.

2. Data and Analyses

Cloud processes are simulated using a one-dimensional (vertical) Lagrangian model driven by meteorological reanalysis temperature field. This approach generally follows the methodology described in Jensen and Pfister (2004), Ueyama et al. (2014, 2015, 2018), and Jensen et al. (2017), but the cloud model was modified to track and record detrained ice crystal properties throughout their lifetimes. We also run a set of idealized simulations to quantify the sensitivity of the detrained ice impact to various parameters. The following sections describe these methods in detail.

2.1. Convectively Influenced Trajectory Calculations

The first step of this study is to calculate 60-day backward diabatic trajectories on 1 February 2007 from a 2° longitude × 2° latitude grid of points in the 30°S to 30°N domain at the 378 K potential temperature level. The 378-K level in boreal winter corresponds to the 93-hPa level near the wintertime cold point

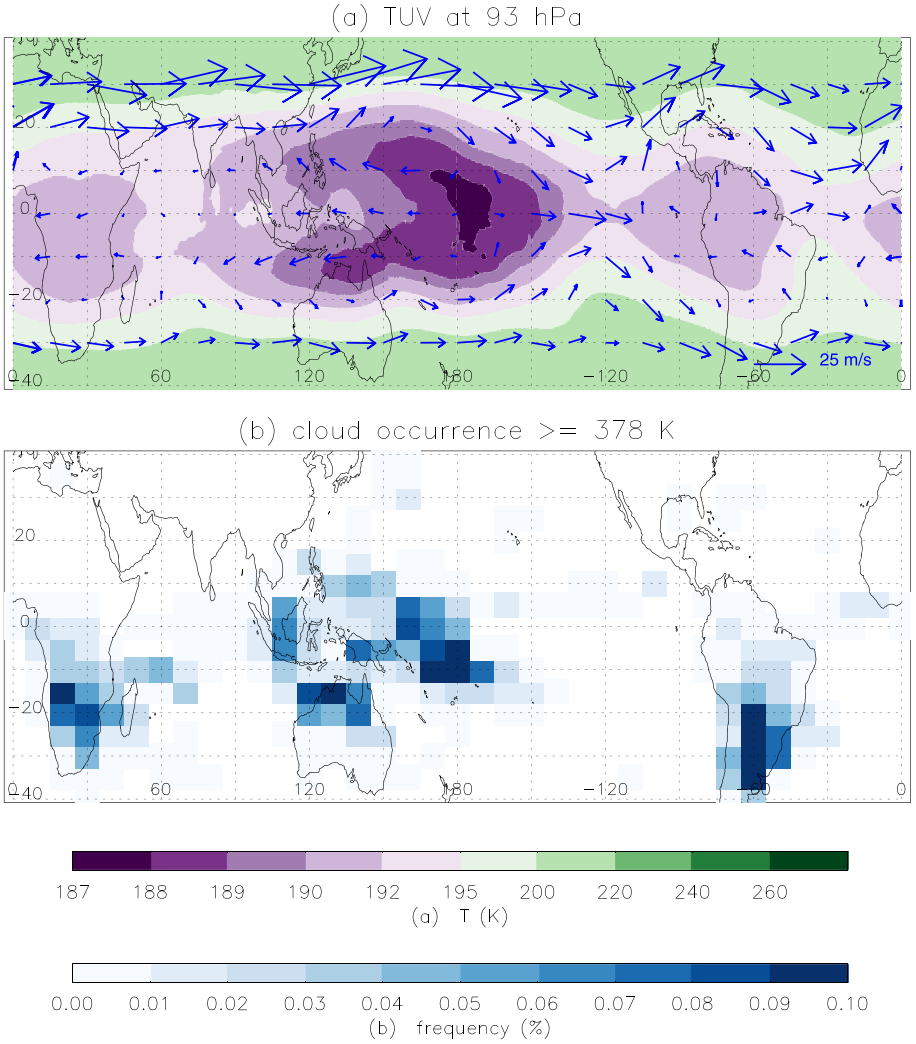

Figure 1. Boreal winter (December 2006 to January 2007) (a) mean temperature (color shading) and wind (vectors) fields at the 93-hPa level from ERA-Interim and (b) occurrence frequencies of deep convective cloud tops ≥ 378 K.

tropopause and is characterized by a region of minimum temperatures in the tropical Pacific centered around the dateline, as shown in Figure 1a. Trajectories are calculated using horizontal wind data from the 6-hourly interim reanalysis of the European Centre for Medium-range Weather Forecasts (ERA-Interim: Dee et al., 2011) and offline radiative-transfer calculations of tropical radiative heating rates (i.e., vertical motion) of Yang et al. (2010) merged with extratropical radiative heating rates from ERA-Interim averaged over the three boreal winter months (December 2006 to February 2007). Although the pathway uncertainties of individual trajectories are large over time scales of weeks, thousands of trajectories are averaged over the tropics to statistically represent the transport characteristics within the TTL (Bergman et al., 2016). The results presented in this study are not sensitive to the day-to-day variability of the backward trajectory starting date (i.e., 29 January to 4 February 2007). As discussed in Ueyama et al. (2015, 2018), the coarse (monthly) temporal resolution of the Yang et al. (2010) heating rates due to the need to aggregate the sparse satellite cloud measurements is a clear disadvantage. However, vertical transport through the TTL is slow (mean ascent rates of approximately 0.3 mm s^{-1} corresponding to a vertical transport time scale through the TTL on the order of 1–2 months), and the cloud impacts on TTL humidity build up over periods of weeks. Radiative heating rate estimates from satellite cloud observations are likely to be more suitable for this study than model-based heating rates (Randel & Jensen, 2013), and thus, we used the monthly mean Yang et al. (2010) heating rates available over the tropics.

We then extract vertical profiles (from the 350- to 430-K potential temperature levels) of ERA-Interim temperatures along each of the trajectories to generate time-height "curtains" of temperature that are used to drive the cloud microphysical model, as explained in section 2.2. An important consideration when calculating the trajectories and generating the temperature curtains is the effect of atmospheric waves that are not resolved in the reanalysis data. To account for this, the interpolation technique of Kim and Alexander (2013) is applied to the ERA-Interim data to recover the degraded wave-driven variability in the TTL. This scheme has been shown to also lower the cold point tropopause temperature by 0.3 K in the tropical mean, which is responsible for lowering the tropical mean, 100-hPa level water vapor mixing ratio by 0.46 ppmv during boreal winter (Ueyama et al., 2015). We note that the ERA-Interim temperatures in the TTL tend to have a slight cold bias of similar magnitude associated with the fast ascent across the tropical tropopause (Dee et al., 2011), but this cold bias will only contribute to the overall model dry bias (see section 3.1) and not affect the results of sensitivity simulations regarding the impact of convection on TTL humidity. High-frequency gravity waves with periods less than 1/2 day are not resolved in the reanalysis data even after applying the Kim and Alexander (2013) interpolation scheme. In general, high-frequency gravity waves have minimal impact on TTL humidity (Fueglistaler & Baker, 2006; Schoeberl et al., 2014, 2015; Ueyama et al., 2015), but they affect cloud microphysical properties such as ice number concentrations and ice crystal size distributions produced by homogeneous ice nucleation (Dinh et al., 2016; Jensen & Pfister, 2004; Schoeberl et al., 2015). High-frequency gravity waves have been shown to increase the occurrence of in situ formed clouds due to their modulation of the cooling rates (Schoeberl et al., 2015, 2016; Ueyama et al., 2015), but the impact of these waves on the detrained ice crystal life cycle is less clear. It is conceivable that these waves could hasten the sublimation of detrained ice in marginally subsaturated environment by permitting complete sublimation of ice crystals in warm phases of the waves that are associated with positive temperature excursions. Here we add the effects of high-frequency gravity waves on TTL temperatures using the gravity wave spectra calculated from pressure perturbations recorded by Project Loon's lower stratospheric superpressure balloons (Schoeberl et al., 2017). The wave amplitudes below the tropopause are attenuated to a value less than half of their tropopause amplitude (i.e., 0.35 K at 15 km) to match the vertical structure of tropical waves analyzed by Kim and Alexander (2013). This study's results using the modified balloon-based gravity wave spectra are similar to those using the climatological mean high-frequency gravity wave spectra described in Jensen and Pfister (2004).

To determine the convective influence of the parcels, trajectories are traced through time-dependent (3-hourly) fields of convective cloud-top height; the time and location (longitude, latitude, and altitude) of convective clouds that intersect each trajectory are recorded (Schoeberl et al., 2018, 2019; Ueyama et al., 2014, 2015, 2018). Convective cloud tops are estimated using global rainfall measurements, geostationary infrared satellite imagery, and temperature analyses (Bergman et al., 2012; Pfister et al., 2001). First, rainfall measurements from Tropical Rainfall Measuring Mission and Global Precipitation Measurement are used to distinguish convective clouds from in situ formed cirrus clouds. Rain rate thresholds used for identification of convection (i.e., 0.9 and 1.5 mm hr^{-1} over land and ocean, respectively) are adjusted to statistically match combined CloudSat and Cloud-Aerosol Lidar with Orthogonal Polarization observations of deep convective cloud-top height frequency. Second, the analysis temperature profiles are modified above the analysis tropopause by calculating a profile that is a mixture of (70%) tropopause air and (30%) environmental air, broadly consistent with the observed cooling effect of convection near the tropopause (Chae et al., 2011; Selkirk, 1993; Sherwood et al., 2003). The altitude of the infrared brightness temperature in the modified temperature profile is then defined as the cloud-top altitude. Lastly, the cloud-top altitudes are adjusted for known biases in infrared cloud-top temperature (Minnis et al., 2008; Sherwood et al., 2004) by uniformly adding 1 km to the cloud-top altitudes. Convective cloud-top heights derived by this methodology capture the extreme deep convective systems that are often underestimated in global model convective parameterizations (e.g., Schoeberl et al., 2018). Proper representation of these deep convective systems that reach the upper TTL and into the lower stratosphere is critical for evaluating the impact of convection and its detrained ice crystals on TTL water vapor and the humidity of air entering the stratosphere.

Figure 1b shows the occurrence frequency of deep convective cloud-top altitudes at or above 378 K during boreal winter 2006–2007. Cloud occurrences are calculated over 10° longitude by 10° latitude grid boxes to increase the sample size within each grid box. Deep convection occurs frequently over the western tropical Pacific to the west of the minimum temperature region, consistent with the relationship between convective

forcing and global-scale temperature response near the tropopause associated with vertically propagating Kelvin waves above the convective region (Randel & Wu, 2005). Winds in this region at the 93-hPa level are weak and easterly in boreal winter 2007, diverging from the minimum temperature region. A pair of anticyclones is observed off of the equator in the western Pacific, straddling the region of deep convection, consistent with the Matsuno-Gill model of steady-state response to a stationary, equatorial heat source (Gill, 1980; Matsuno, 1966). Besides the western tropical Pacific, deep convective cloud tops are also observed frequently in smaller regions over northern Australia, southern Africa, and South America.

2.2. Cloud Microphysical Model and Detrained Ice Tracking

Time-height "curtains" of temperature and heating rate are used to drive the one-dimensional (column) cloud microphysical model that simulates cloud ice processes such as nucleation, deposition growth, sedimentation, and sublimation along the trajectories between 350- and 430-K potential temperature levels. Homogeneous ice nucleation is triggered when the relative humidity with respect to ice (i.e., ice saturation ratio) exceeds a threshold of ~1.6 (Koop et al., 2000). Heterogeneous ice nucleation that occurs at moderate supersaturations is not included in these simulations, but Ueyama et al. (2015) have shown that the effect of heterogeneous nucleation (as opposed to homogeneous nucleation) on TTL water vapor is small: dehydration effect of 0.05 ppmv in the tropical mean at the 100-hPa level in boreal winter. The model tracks the sizes and heights of thousands of individual ice crystals to represent clouds. Ice crystals are assumed to be in thermal equilibrium with the ambient air. Water vapor is treated using an Eulerian grid, and the water exchange between the vapor and condensed phases is computed. Vertical advection of water vapor and ice crystals is diagnosed using the heating rate curtains. The model is initialized with the 7-day mean Microwave Limb Sounder (MLS) water vapor profile averaged over the 5° longitude × 5° latitude grid box nearest to the parcel location at the earliest day of the trajectory, though the results are not sensitive to the initial water vapor distribution. The typical single-profile precision of the water vapor measurements at the 100-hPa level is 15% with an accuracy of 8% (Livesey et al., 2015; Read et al., 2007). The lack of vertical wind shear of the curtain approach is a limitation, but this approach has been used successfully to simulate TTL cirrus and water vapor (e.g., Jensen et al., 2005, 2010, 2012, 2017; Ueyama et al., 2014, 2015, 2018) as well as midlatitude cirrus (Jensen et al., 2013).

Whenever a trajectory intersects a convective cloud, the column model with a vertical range of 350–430 K is saturated up to the cloud-top potential temperature. In other words, if the atmosphere is initially subsaturated (supersaturated), convective influence will increase (decrease) the relative humidity. Additionally, monodispersed ice crystals of diameter 30 μm with an ice water content of 30 ppmv are added to the column model up to the cloud-top potential temperature to simulate the anvil cirrus detrained from deep convection. We will examine the sensitivity of TTL water vapor to anvil ice crystal sizes and ice water content within the range of available aircraft measurements (Frey et al., 2011, 2014, 2015; Jensen et al., 2009; Krämer et al., 2020), as described in the next section. As mentioned above, thousands of individual ice crystals are tracked. The changes in the radius, potential temperature, temperature, water vapor, and ice saturation ratio of each ice crystal are recorded throughout its lifetime. The cumulative impact of all detrained ice crystals on TTL water vapor during boreal winter is quantified by calculating the difference between the water vapor profiles on the final day (i.e., start date of the backward trajectories) of the simulations with and without detrained ice. The results are discussed in section 3.

2.3. Idealized Simulations for Sensitivity Tests

In order to investigate the sensitivity of TTL water vapor to various parameters such as downstream temperature tendency and detrained ice crystal sizes, we also run several sets of idealized simulations. We start with a typical tropical sounding temperature profile and set the relative humidity below 375 K to 100%. Ice crystals of given size and ice water content are then injected up to the 375-K level shortly after the beginning of the simulation. We also test the sensitivity of TTL water vapor to variable-sized detrained ice crystals using the ice size distribution measurements collected in the fresh convective outflow at 17.5 km during the 10 August flight of the StratoClim campaign (Krämer et al., 2020). The StratoClim ice size distribution includes relatively abundant small (diameter < 30 μm) ice crystals (Figure 2), but the mass is dominated by large crystals. Following the ice injection, we impose a constant heating/cooling rate at each potential temperature level. In this setup, the imposed heating and cooling represent the transport of air parcels along constant potential temperature surfaces that slope upward/downward; diabatic (radiative) heating is not involved.

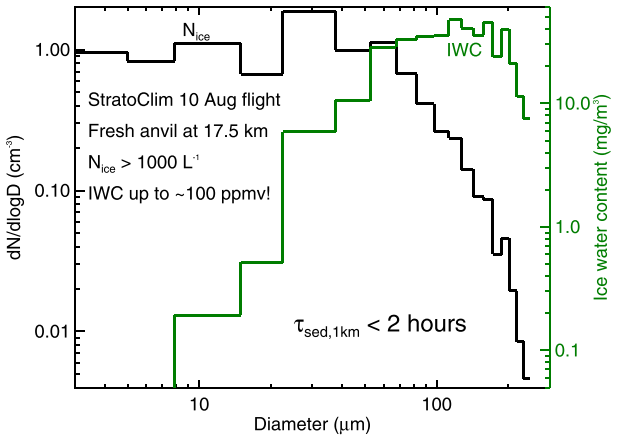

Figure 2. Number concentration and ice water content of ice particles in the fresh anvil at 17.5 km sampled during 10 August flight of the StratoClim campaign.

Each simulation is run for up to 10 days, and the change in the water vapor profile is calculated. The simulation length depends on the sedimentation time scale of the ice crystals, which is longer for smaller ice crystals.

For calculation of ice crystal sedimentation speeds, we use the approach described by Heymfield and Westbrook (2010). Sedimentation speed depends on the crystal shape. Given the limits of airborne ice crystal imaging instruments, shapes of crystals with maximum dimensions smaller than about 50-μm diameter are not known (Lawson et al., 2008). Larger crystals are found to be pristine shapes or aggregates in fresh anvils, whereas in aged anvils, bullet rosettes tend to dominate (Lawson et al., 2019). We have assumed spheres in our calculations, which result in the maximum possible sedimentation speeds. Ice crystal shapes are generally parameterized with power law expressions relating the crystal mass and area to maximum dimension. Using the power law parameters provided by Sölch and Kärcher (2010, and references therein) for aggregates and bullet rosettes, the sedimentation speeds are only moderately (<30%) reduced for the assumed monodispersed crystals with spherical-equivalent diameters less than the 60 μm value used in our calculations. For the larger crystals included in the size distribution taken from the StratoClim measurements (Krämer et al., 2020), the shape effect on sedimentation speed can be up to a factor of 2, but the larger crystals tend to sediment out relatively quickly (see section 3.3). Smaller sedimentation speeds would allow more time for the ice to grow/sublimate in cases with cooling/heating downstream of the convection. Therefore, the assumption of spherical shapes used here provides the minimum impact of detrained ice on water vapor. Assuming aggregates or bullet rosettes in the idealized simulations with monodispersed ice crystals increases the impact of detrained ice on TTL water vapor by about 10–30%.

3. Results

3.1. Tropical Mean Impact of Convection on TTL Water Vapor

The 100-hPa level water vapor mixing ratios in the tropics on 1 February 2007 as measured by MLS are shown in Figure 3a. It is characterized by a broad region of dry (~2 ppmv) air in the western tropical Pacific. The eastern tropical Pacific is also relatively dry compared to the zonal mean but not as dry as the western Pacific basin. These dry regions are surrounded by relatively moist air in the subtropics, reminiscent of the structure of the 93-hPa level temperature field in Figure 1a. It is well known that water vapor and temperature fields are well correlated at these TTL levels (Mote et al., 1996; Randel & Jensen, 2013; Randel & Park, 2019; Randel et al., 2004) due to the freeze drying of air during its passage through the cold point tropopause. A careful comparison of the 100-hPa water vapor field (Figure 3a) and the 93-hPa temperature field (Figure 1a) however reveals some differences in their spatial patterns. For example, the region of minimum water vapor over the western Pacific is shifted westward from the minimum temperature region centered near the dateline, presumably due to the westward transport of dehydrated air by the diverging, easterly flow. The water vapor field also exhibits larger spatial variability than the temperature field. The sparse nature of MLS measurements certainly contributes to the spatial variance of the 100-hPa water vapor field shown in Figure 3a, but deep convection penetrating the TTL (Figure 1b) also modulates the water vapor distribution, as described below.

Figure 3b shows the reference curtain model simulation with the full effect of convection, including the effect of near-instantaneous convective saturation as well as the delayed impact of detrained ice crystals in aging anvils. Whenever a trajectory intersects a convective cloud, the column model is instantaneously saturated up to the cloud-top potential temperature, and monodispersed ice crystals of diameter 30 μm with an ice water content of 30 ppmv are added. The MLS averaging kernel is applied to the simulated water vapor profiles at each 2° longitude × 2° latitude grid point before averaging over 5° longitude × 5° latitude grid boxes. The simulated water vapor field resembles the observed field with dry regions over the western and eastern tropical Pacific surrounded by the moist subtropics. The north-south-oriented strip of dry air

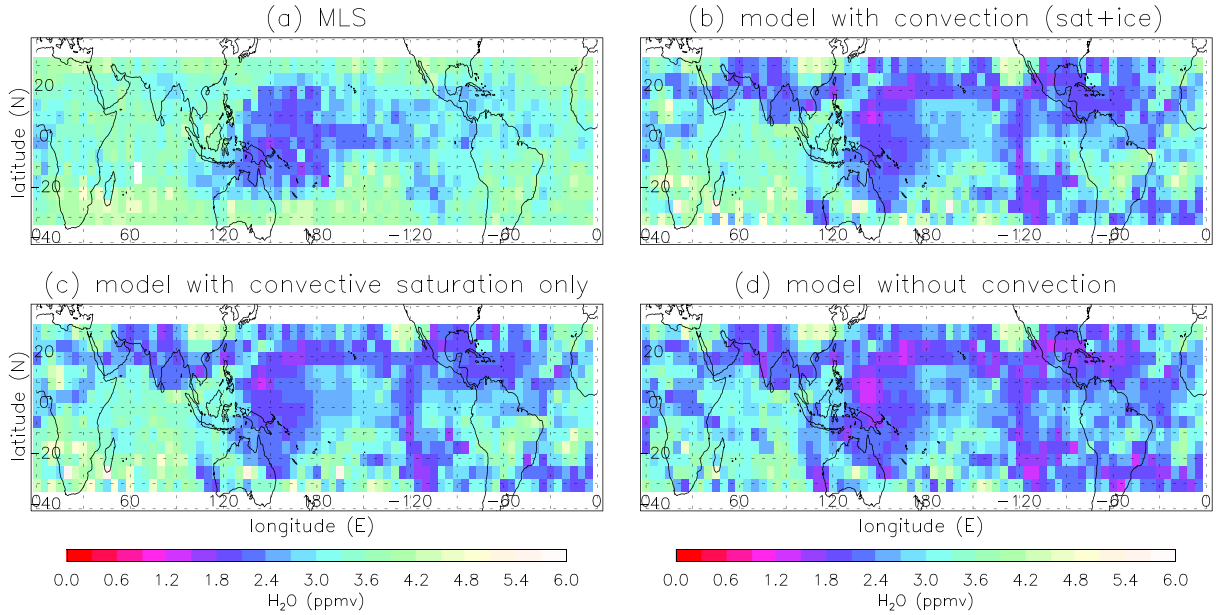

Figure 3. (a) Seven-day mean 100-hPa level MLS H_2O centered on 1 February 2007. Simulated 100-hPa level H_2O (b) with the full effect of convection including convective saturation and convectively detrained ice, (c) with convective saturation but no detrained ice, and (d) without convective saturation or convectively detrained ice. See text for details.

along 120°W is evident in both the simulated and observed fields, but it is more prominent in the model. The dry air over the western Pacific is displaced northward in the model rather than being centered on the equator. The northern subtropics are also generally too dry compared to observations, which could be due to the lack of horizontal in-mixing of relatively moist air from the extratropics in the model.

To investigate the impact of convection on TTL water vapor, the model is run two more times with adjustments to the convective parameters. Figure 3c represents the 100-hPa level water vapor field in the simulation with convective saturation but without the detrainment of ice crystals. Figure 3d represents the 100-hPa level water vapor field in the simulation without convection (i.e., neither the effects of saturation nor detrained ice are included). The difference between the simulated fields with and without convective saturation (Figure 3c minus Figure 3d), shown in Figure 4a, indicates that the saturating effect of convection moistens the 100-hPa level by about 0.30 ppmv in the tropical mean, consistent with previous studies (Schoeberl et al., 2018; Ueyama et al., 2015, 2018). In contrast, a close resemblance between the simulated fields with and without detrained ice (Figures 3b and 3c) suggests that detrained ice has a negligible impact on the water vapor mixing ratios at the 100-hPa level. The difference field shown in Figure 4b indicates that the impact of

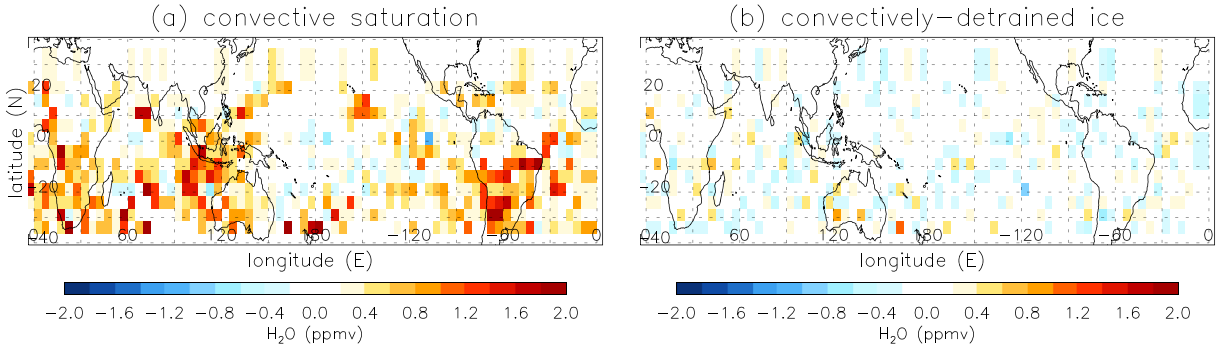

Figure 4. Impact of (a) convective saturation and (b) convectively detrained ice on 100-hPa level H_2O calculated as differences between two simulations Figures 3c and 3d for (a) and Figures 3b and 3c for (b). MLS averaging kernel is not applied when calculating the differences between two simulated fields.

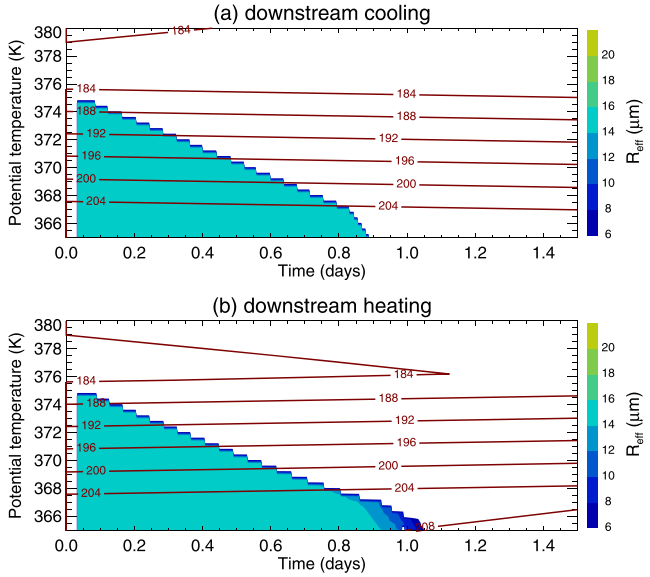

Figure 5. Time versus potential temperature "curtain" plots of temperature (contours) and effective radius of detrained ice crystals with ice water content >0 (color shading) from idealized simulations with downstream (a) cooling and (b) heating of 1 K day^{-1}. Monodispersed ice crystals of diameter 30 μm and ice water content of 30 ppmv are injected up to the 375-K level shortly after the beginning of the simulation. See text for details.

detrained ice is in fact a slight *dehydration* of 0.01 ppmv in the tropical mean at the 100-hPa level as well as the 83-hPa level (not shown). In other words, the effect of convective saturation is significantly larger than the dehydration effect of detrained ice.

3.2. Role of Downstream Temperature Tendency and Saturation

A possible explanation for the dehydrating effect of convectively detrained ice crystals is that the ice crystals encounter supersaturated environment downstream of convection such that vapor in excess of saturation condenses on the ice crystals (Jensen et al., 2007). The ice crystals grow and sediment out of the TTL, effectively lowering the relative humidity with respect to ice and dehydrating the TTL. Supersaturated air may be found downstream of deep convection presumably because air is ascending at these levels and thus is cooling. In our simulations, the column model is saturated up to the cloud-top level at every convective encounter, so ascent and cooling downstream of convection will increase relative humidity above 100%. The terminologies "cooling" and "heating" in this study refer to temperature changes experienced by parcels due to their ascent and descent, respectively, and not by diabatic motions. Cloud radiative heating is not included.

We investigate this hypothesis by first examining the impact of downstream temperature tendency (dT/dt) on the ice saturation ratios and water vapor mixing ratios in the TTL in a set of idealized simulations described in section 2.3. Figure 5 shows time-height curtains of temperature and ice saturation ratios for the idealized simulations with imposed cooling and heating of 1 K day^{-1} at all potential temperature levels between 365 and 380 K. Colored shading represents the evolution of the effective radius of detrained ice injected at Day 0. As expected, the TTL below the convective cloud-top potential temperature of 375 K becomes supersaturated when the cooling causes the temperature to decrease downstream of convection. Ice crystals grow rapidly, and all of the ice falls below the model domain within a day. In contrast, downstream warming of the air parcels produces subsaturated TTL that allows detrained ice crystals to persist slightly longer due to the smaller fall speeds of sublimating ice crystals. In both cases, the change in ice crystal size is minimal, and sedimentation of ice crystals dominates the ice crystal loss process in these simulations where ice growth and sublimation are limited by the large reservoir of ice that maintains saturation.

The impact of detrained ice on TTL water vapor mixing ratios for the downstream cooling and warming cases is summarized in Figure 6: When the imposed temperature tendency is negative (positive), ice crystals have a dehydrating (moistening) effect below the detrainment level. In other words, detrained ice crystals that encounter cooler temperatures (and thus supersaturated air) will leave behind air that is less humid than before, whereas those that encounter warmer temperatures (and thus subsaturated air) will sublimate and hydrate the layers below the detrainment level. Note however that the net dehydration and hydration effects are relatively small for small changes in temperature (i.e., a few percent or 0.05 ppmv change in water vapor at ~370 K with a mean water vapor mixing ratio of ~3 ppmv for dT/dt of 0.5 K day^{-1}). Since the sedimentation speeds of the ice crystals are comparable in the heating and cooling simulations (Figure 5), the change in water vapor is approximately equal and opposite in the sets of heating and cooling simulations (Figure 6).

Given the sensitivity of the water vapor concentrations to downstream temperature tendency in the idealized simulations, we explore the temperature tendencies downstream of convection along the convectively influenced trajectories. Figure 7 shows the temperature tendencies downstream of deep convective cloud tops (>370 K) along the trajectories averaged over the 10-K layer below the convective cloud-top potential temperature. The time interval (dt) of 1 day is used to calculate the temperature tendency. For example, when a trajectory intersects a convective cloud top of 375 K, the temperature tendency following the trajectory over a 1-day period averaged over the 365- to 375-K layer is computed. We exclude convective events occurring multiple times within a day of each other since the objective is to investigate the magnitude of

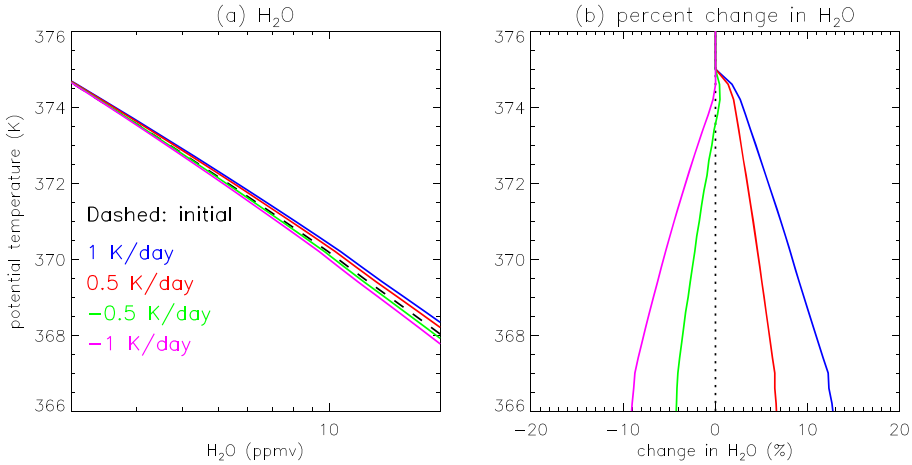

Figure 6. (a) Vertical profiles of H_2O in a set of idealized simulations with different temperature tendencies: heating rate of 1 and 0.5 K day^{-1} (blue and red) and cooling rate of 1 and 0.5 K day^{-1} (magenta and green). (b) Vertical profiles of the percent change in H_2O associated with the impact of downstream temperature tendency on the detrained ice crystal evolution.

the heating or cooling downstream of deep convection during a 1-day period following a convective influence event. The peak of the probability density function is centered near zero, indicating that over the course of a day, detrained ice crystals experience only a small change in temperature from the time of convective detrainment (blue, Figure 7a). The mean temperature tendency downstream of convection is a slight cooling of 0.45 K day^{-1}. In contrast, the average temperature tendency in the 360- to 370-K layer over nonconvective regions is a slight heating of 0.24 K day^{-1} (red, Figure 7a). The isentropic cooling and heating rates on the order of 1 K day^{-1} are larger than the typical diabatic heating rates in the TTL.

The temperature tendencies downstream of all convective influence events above 370 K are averaged over the 5° latitude × 5° longitude grid in Figure 7b. Not surprisingly, convective influence locations resemble the pattern of frequent deep convection (Figure 1b) with four centers of convective activity in the tropical western Pacific and Maritime Continent, northern Australia, southern Africa, and South America. There

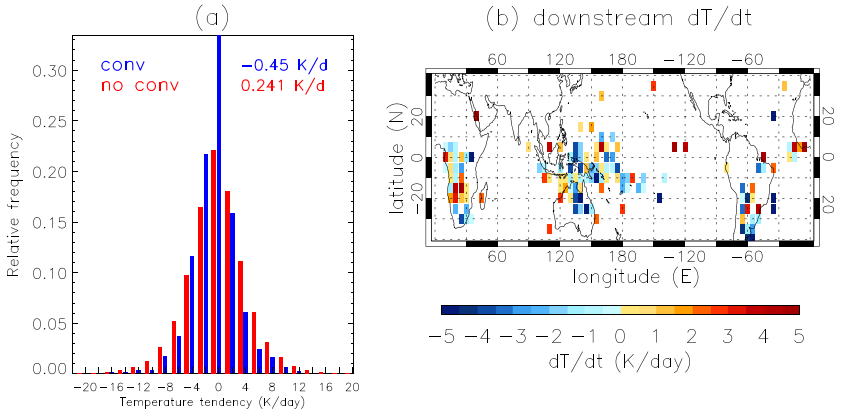

Figure 7. (a) Frequency distributions of the temperature tendency (dT/dt) downstream of deep convection (cloud top > 370 K) calculated as the change in the 10-K layer mean temperature below the convective cloud-top potential temperature level over a 1-day period (dt = 1 day) (blue). Frequency distributions of dT/dt in nonconvective regions averaged over the 360- to 370-K layer (red). The mean of the frequency distributions over convective and nonconvective regions is −0.45 and +0.24 K day^{-1}, respectively. (b) Map of the downstream temperature tendencies averaged over 5° latitude × 5° longitude grid boxes. These calculations are based on convectively influenced 60-day backward trajectories launched from the tropics on 1 February 2007 near the wintertime cold point tropopause (378-K potential temperature level).

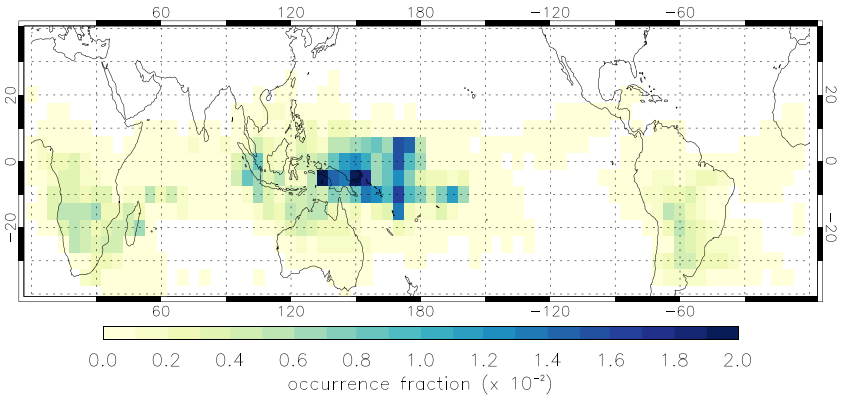

Figure 8. Occurrence frequencies of convectively detrained ice crystals in the tropical tropopause layer (370–400 K) during boreal winter 2007 based on convectively influenced 60-day backward trajectories launched from the tropics on 1 February 2007 near the wintertime cold point tropopause (378-K potential temperature level).

is considerable regional variability as well as variability within each of these regions. Nonetheless, the tropical western Pacific and Maritime Continent stand out as a region of predominant cooling of up to 5 K day^{-1}. Detrained ice crystals are also most frequently observed there, as shown in Figure 8. Approximately 40% of convectively influenced parcels that arrive at the 378-K level in the tropics during boreal winter are influenced by convection over the western Pacific. The ice saturation ratio encountered by ice crystals detrained from western Pacific convection, shown in Figure 9, indicates slight supersaturation at levels below ~380 K, consistent with the downstream cooling. Since convective cloud-top occurrence frequency, and therefore the detrained ice occurrence frequency, decreases rapidly with increasing altitude, the statistical significance of the mean ice saturation ratios in Figure 9 decreases with increasing altitude in the TTL. The saturation ratios do not deviate much from unity because the air is saturated whenever convection is encountered (see section 2.2) and the subsequent ice growth or sublimation maintains the saturation ratio close to unity. These results are consistent with the theoretical understanding of the convective impact on TTL humidity discussed in section 1: Downstream cooling and supersaturation allow vapor in excess of saturation to condense on the detrained ice crystals and thus lead to dehydration, as found in Figure 4b. The dehydration effect of detrained ice on the 100-hPa level does not maximize over the western Pacific (Figure 4b) where detrained ice crystals are abundantly found (Figure 8) because parcels influenced by western Pacific convection do not necessarily stay within the western Pacific region before arriving at the 378-K level. The detrained ice effect associated with western Pacific convection would manifest itself in regions outside of the western Pacific in Figure 4b, if the convectively influenced parcel is subsequently transported away from this convective region.

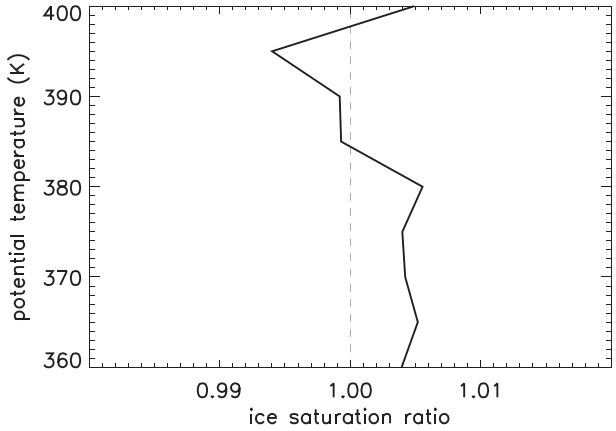

Figure 9. Vertical profile of mean ice saturation ratio experienced by convectively detrained ice crystals downstream of western Pacific (10°S to 5°N, 140–180°E) convection in the tropical tropopause layer (370–400 K) during boreal winter 2007.

3.3. Idealized Simulations for Sensitivity Tests

Our simulation assumes that whenever a trajectory is influenced by convection, the atmosphere becomes saturated up to the cloud-top potential temperature by the upward transport of boundary layer air and/or near-instantaneous sublimation of ice crystals that have been lofted by convection. We also assume that monodispersed ice crystals of diameter 30 μm and an ice water content of 30 ppmv are left behind after the active convective anvil has subsided, which we have been referring to as detrained ice. Here, we investigate the sensitivity of the water vapor impact to the size and ice water content of detrained ice in a set of idealized simulations.

As shown in Figure 10, water vapor below the detrainment level shows weak sensitivity to the ice water content of detrained ice in both cooling and heating scenarios (red lines). Essentially, so long as sufficient ice mass is present, the change in vapor pressure driven by cooling/heating is

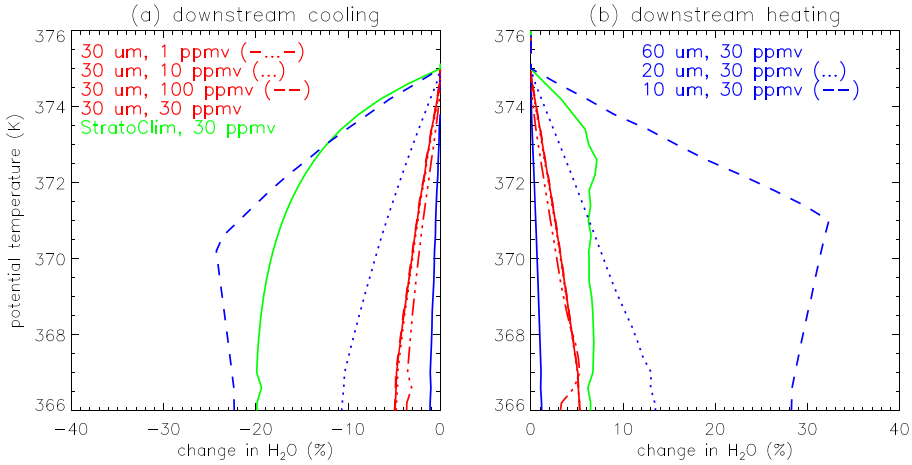

Figure 10. Vertical profiles of the percent change in H_2O associated with the impact of downstream (a) cooling and (b) heating of 0.5 K day^{-1} on the detrained ice crystals in a set of idealized simulations with varying ice water content (IWC) and sizes: (red) ice crystal diameter of 30 μm and varying IWC of 30 ppmv (solid), 1 ppmv (dash-dot-dot-dot), 10 ppmv (dot), and 100 ppmv (dash); (blue) IWC of 30 ppmv and varying ice crystal diameter of 60 μm (solid), 20 μm (dot), and 10 μm (dash); and (green) StratoClim particle size distribution and IWC of 30 ppmv.

balanced by ice growth or sublimation, but the change in ice water content is small, and most of the ice falls out of the TTL. In contrast, the water vapor impact exhibits strong sensitivity to decreasing ice crystal size (blue lines). With a relatively slow heating rate of 0.5 K day^{-1}, large ice crystals (diameter > 50 μm) fall out quickly and therefore do not contribute much to the change in water vapor mixing ratio. Indeed, water vapor changes in the simulation with monodispersed ice crystals of diameter 60 μm are about one fifth of those in the simulation with diameter 30 μm ice crystals and an order of magnitude less than those in the simulation with diameter 20 μm ice crystals. In general, the sizes of small ice crystals change very little as a result of slow heating or cooling on the order of 1 K day^{-1} (Figure 5), and the saturation ratio does not deviate very far from unity. Since the supersaturations/subsaturations are small, changes in water vapor in the cooling simulations are approximately equal and opposite to those in heating simulations (see also Figure 6). This result is consistent with the theoretical understanding that the Clausius-Clapeyron expression is approximately linear for small changes in temperature. However, a closer inspection of Figure 10 reveals that as ice crystal size decreases, moistening by the sublimation of ice crystals in the heating simulation becomes larger than the dehydration by the deposition growth of ice crystals in the cooling simulation. This occurs because sedimentation rate of sublimating ice crystals in the heating simulation is slightly slower than the sedimentation rate of growing ice crystals in the cooling simulation.

The interpretation of the results of the idealized simulations using StratoClim particle size distribution with ice crystal diameter ranging from approximately 10 to 100 μm (Figure 2) is more complicated. Compared to the simulations with monodispersed ice crystals, the difference between the cooling and heating simulations is stark (green lines). Water vapor changes are larger in a cooling environment than in a heating environment (i.e., 10% or 0.3-ppmv decrease vs. 5% or 0.15-ppmv increase in water vapor at ~370 K with a mean water vapor mixing ratio of ~3 ppmv for 0.5 K day^{-1} cooling and heating, respectively) because of the longer lifetime of an ice cloud in the presence of cooling. This seemingly contradicts the results from the idealized simulations with monodispersed ice crystals where the cloud persists slightly longer in a heating environment than in a cooling environment because of the slightly slower sedimentation of sublimating ice crystals in the heating simulation. In the monodispersed simulations, the cloud lifetime is primarily determined by the sedimentation time scale. In contrast, ice growth and sublimation play a more important role in the evolution of the cloud and water vapor in the simulations with StratoClim particle size distribution. This is because the large ice crystals (diameter > 20 μm) in the StratoClim particle size distribution that contain most of the ice mass are quickly lost via sedimentation in both the heating and cooling simulations. After about a day, only the small ice crystals (diameter < 20 μm) with relatively low ice water content remain.

These small ice crystals can readily grow or sublimate as cooling or heating continues. The combination of rapid sedimentation (of large ice crystals) followed by rapid sublimation (of small ice crystals) results in a relatively short lifetime of the cloud in the heating simulation. The cloud in the cooling simulation lasts much longer because the small ice crystals grow to about 10 to 30 μm before they fall out and, therefore, continue to deplete the vapor long after the ice cloud in the heating simulation is gone.

4. Summary and Discussion

This study is aimed at quantifying the impact of convectively detrained ice crystals on the humidity of the TTL during boreal winter 2007 using one-dimensional (vertical) simulations of TTL clouds and water vapor along convectively influenced trajectories. The 60-day backward trajectories are launched from the tropics at the 378-K potential temperature (93-hPa pressure) level on 1 February 2007 and traced through global, 3-hourly satellite-derived convective cloud-top altitude fields to determine the convective influence of parcels along their trajectories. While the satellite-derived convective cloud tops used in this study are likely of a variety of ages, we assume that all convective influence events are associated with relatively aged anvil cirrus in which the primary physical processes are ice sedimentation and deposition growth or sublimation. Whenever a trajectory intersects a convective cloud, the atmospheric column is saturated up to the convective cloud-top potential temperature. Additionally, to simulate the effect of anvil cirrus detrained from deep convection, ice crystals are added to the column microphysical model up to the convective cloud-top potential temperature. If the atmosphere is initially subsaturated (supersaturated), at least some of the ice lofted from convection will sublimate (grow via deposition) relatively quickly to establish or maintain saturation of the convective environment. The active convective core and fresh anvil typically subside in a few hours, leaving behind some ice crystals in an aging cirrus anvil, which we refer to as detrained ice. The focus of this study is on these detrained ice crystals that can carry the effect of convection some distance downstream of the convection and impact the TTL humidity long after the convective event has occurred.

Comparison between simulations with and without detrained ice indicates that convectively detrained ice crystals slightly dehydrate (0.01 ppmv) the tropics at the 378-K level (Figure 4b). This is because detrained ice crystals, most of which are found over the western Pacific (Figure 8), predominantly experience cooling (an average cooling of 0.5 K day^{-1} but locally as large as 4–5 K day^{-1}) downstream of convection (Figure 7). Supersaturated air is found downstream of deep convection over the western Pacific (Figure 9) presumably because air is ascending at these levels and thus is cooling. In such an environment, vapor in excess of saturation condenses onto the detrained ice crystals which ultimately brings the relative humidity down to saturation (i.e., dehydration). When the ice crystals become large enough, they fall to lower levels where they often encounter subsaturated air and sublimate. Thus, the overall effect of detrained ice crystals on the wintertime TTL is a slight dehydration followed by hydration at lower levels.

Sensitivity simulations in the idealized cloud model with a typical tropical sounding temperature profile and detrained ice crystals of a specified size and ice water content indicate that TTL humidity is not sensitive to the ice water content of detrained ice crystals (Figure 10). The detrained ice impact on TTL humidity is however sensitive to ice crystal size. Large ice crystals fall out quickly and therefore do not have a large influence on water vapor. In comparison, small ice crystals show greater sensitivity to the temperature changes downstream. The simulation using a realistic particle size distribution of detrained ice crystals based on StratoClim campaign measurements (Figure 2) exhibits larger water vapor changes in a cooling environment than in a heating environment because of the relatively long lifetime of the ice cloud in the presence of cooling. A full, global simulation with StratoClim particle size distribution indicates that ice crystals detrained from western Pacific convection predominantly dehydrate the 378-K level (not shown), similar to the results shown here using monodispersed ice crystals of diameter 30 μm. In general, the dehydration effects of detrained ice in a downstream cooling environment nearly cancel the hydration effects of detrained ice in a downstream warming environment in both the simulations using monodispersed ice crystals and StratoClim particle size distribution.

The main result is that moistening of the TTL by the active convective core, including the rapid sublimation of convectively lofted ice crystals in fresh anvils, is an order of magnitude larger than the dehydrating effect of detrained ice crystals in aging anvils. The net effect is moistening by convective core anvils during boreal winter. Detrained ice primarily dehydrates the TTL because the temperature tendency encountered by the

detrained ice downstream of convection exhibits substantial regional variability with an average cooling on the order of 1 K day^{-1} (Figure 7). We have not included mesoscale dynamics driven by the convection and cloud-scale motions driven by cloud radiative heating in our model, which could lead to significant temperature variability. This temperature variability will presumably be transient, with the anvil temperature eventually relaxing back to the large-scale environmental temperature. However, significant warming in the near field could drive ice sublimation and hydration that are not included here.

A similar study by Ueyama et al. (2015) found a 0.55-ppmv moistening effect of detrained ice on the water vapor at the 372-K potential temperature (100-hPa pressure) level during boreal winter 2007. They used the same definition of "detrained ice" as this study. Several modifications to the ice injection methodology in the cloud model such as specifying a fixed ice water content instead of the number concentration may have contributed to the different results. However, we note that the slight dehydration effect of detrained ice crystals found in this study is consistent with the theoretical understanding of cloud microphysical processes in a cooling and supersaturated environment. The detrained ice impact was not the focus of Ueyama et al. (2015) study and therefore was not investigated in detail. We also expect a smaller effect of detrained ice in the current model setup compared to that of Ueyama et al. (2015) because the detrained ice size is larger (diameter of 30 vs. 20 μm, more in agreement with anvil ice crystal measurements from StratoClim) and the trajectories are launched at a higher potential temperature (378 vs. 372 K) where convective occurrence is less frequent.

The apparent discrepancy between our study's results and those of other studies that noted a significant moistening of the TTL by convectively lofted ice crystals (e.g., Avery et al., 2017; Dessler et al., 2007, 2016; Ye et al., 2018) is primarily because of the different definitions of the detrained ice effect in these studies. The studies that found a large effect of "detrained ice" on TTL humidity assumed that the convectively influenced environment is instantaneously moistened by the sublimation of convectively lofted ice crystals; these studies neglect the impact of detrained ice crystals that remain after the active convection has subsided. In some sense, the distinction between the effects of instantaneous saturation (i.e., moistening by the active convective core and fresh anvils) and longer-lasting detrained ice crystals in aging anvils is moot because the latter effect is very small. Upward transport of boundary layer air and/or near-instantaneous sublimation of convectively lofted ice in a subsaturated TTL air dominates the total convective impact. However, we argue that this distinction is important because there is evidence of detrained ice crystals existing away from active convection and above the cold point tropopause (Corti et al., 2008; Nielsen et al., 2007; Schiller et al., 2009). Future changes in convective activity could involve changes in the abundance of detrained ice crystals near the cold point tropopause and the relative importance of detrained ice on TTL humidity.

We have also shown that accurate representations of ice crystal sizes and downstream temperature tendencies experienced by the detrained ice crystals throughout their lifetimes are necessary for quantifying the regional differences in the impact of convection on TTL humidity. This study focuses on the impact of convection on the TTL water vapor budget near the wintertime cold point tropopause, but our results likely include some incidences of ice sublimation in the lower stratosphere. We note that the impact of detrained ice crystals on TTL humidity may be different during boreal summer due to differences in convective cloud-top distribution and the environment into which ice crystals are detrained. In particular, ice crystals detrained from deep summertime convection over the North American monsoon region are likely to sublimate rapidly as discussed in Ueyama et al. (2018) and therefore potentially moisten the lower stratosphere (Smith et al., 2017). Convective impacts on the humidity of air in the lower stratosphere during boreal winter and summer will be specifically addressed in a follow-up study.

Data Availability Statement

The satellite and reanalysis data used in this study were publicly obtained from the following websites: MLS (https://mls.jpl.nasa.gov/), CALIOP (https://eosweb.larc.nasa.gov/project/calipso/calipso_table), TRMM/GPM rainfall (https://disc.gsfc.nasa.gov/datasets/TRMM_3B42_7/summary?keywords=TRMM%20GPM), and ERA-Interim (https://apps.ecmwf.int/datasets/data/interim-full-daily/levtype=ml/). Our cloud model data are available online (https://bocachica.arc.nasa.gov/rueyama/pubs/2020_detice/). NASA Ames convective cloud-top altitude data are available online (https://bocachica.arc.nasa.gov/nasaarc_cldalt/).

Acknowledgments

This work was supported by NASA grants in the Upper Atmospheric Composition Observations, Aura Science Team and Atmospheric Composition Modeling and Analysis Program, and SAGE III/ISS Science Team programs as well as with funding from the Atmospheric Composition Program through the NASA Internal Scientist Funding Model. We thank Wiebke Frey and two anonymous reviewers for suggestions and constructive comments on the manuscript.

References

Avery, M. A., Davis, S. M., Rosenlof, K. H., Ye, H., & Dessler, A. E. (2017). Large anomalies in lower stratospheric water vapour and ice during the 2015-2016 El Niño. *Nature Geoscience*, *10*(6), 405–409. https://doi.org/10.1038/NGEO2961

Bergman, J. W., Jensen, E. J., Pfister, L., & Bui, T. V. (2016). Air parcel trajectory dispersion near the tropical tropopause. *Journal of Geophysical Research: Atmospheres*, *121*, 3759–3775. https://doi.org/10.1002/2015JD024320

Bergman, J. W., Jensen, E. J., Pfister, L., & Yang, Q. (2012). Seasonal differences of vertical-transport efficiency in the tropical tropopause layer: On the interplay between tropical deep convection, large-scale vertical ascent, and horizontal circulations. *Journal of Geophysical Research*, *117*, D05302. https://doi.org/10.1029/2011JD016992

Bonazzola, M., & Haynes, P. H. (2004). A trajectory-based study of the tropical tropopause region. *Journal of Geophysical Research*, *109*, D20112. https://doi.org/10.1029/2003JD004356

Brewer, A. M. (1949). Evidence for a world circulation provided by the measurements of helium and water vapor distribution in the stratosphere. *Quarterly Journal of the Royal Meteorological Society*, *75*(326), 351–363. https://doi.org/10.1002/qj.49707532603

Chaboureau, J.-P., Cammas, J.-P., Duron, J., Mascart, P. J., Sitnikov, N. M., & Voessing, H.-J. (2007). A numerical study of tropical cross-tropopause transport by convective overshoots. *Atmospheric Chemistry and Physics*, *7*(7), 1731–1740. https://doi.org/10.5194/acp-7-1731-2007

Chae, J. H., Wu, D. L., Read, W. G., & Sherwood, S. C. (2011). The role of tropical deep convective clouds on temperature, water vapor, and dehydration in the tropical tropopause layer (TTL). *Atmospheric Chemistry and Physics*, *11*(8), 3811–3821. https://doi.org/10.6194/acp-11-3811-2011

Corti, T., Luo, B. P., de Reus, M., Brunner, D., Cairo, F., Mahoney, M. J., et al. (2008). Unprecedented evidence for deep convection hydrating the tropical stratosphere. *Geophysical Research Letters*, *35*, L10810. https://doi.org/10.1029/2008GL033641

Danielsen, E. F. (1982). A dehydration mechanism for the stratosphere. *Geophysical Research Letters*, *9*(6), 605–608. https://doi.org/10.1029/GL009i006p00605

Danielsen, E. F. (1993). In situ evidence of rapid, vertical, irreversible transport of lower tropospheric air into the lower tropical stratosphere by convective cloud turrets and by larger-scale upwelling in tropical cyclones. *Journal of Geophysical Research*, *98*(D5), 8665–8681. https://doi.org/10.1029/92JD02954

Dee, D. P., Uppala, S. M., Simmons, A. J., Berrisford, P., Poli, P., Kobayashi, S., et al. (2011). The ERA-interim reanalysis: Configuration and performance of data assimilation system. *Quarterly Journal of the Royal Meteorological Society*, *137*(656), 553–597. https://doi.org/10.1002/qj.828

Dessler, A. E., Hanisco, T. F., & Fueglistaler, S. (2007). Effects of convective ice lofting on H_2O and HDO in the tropical tropopause layer. *Journal of Geophysical Research*, *112*, D18309. https://doi.org/10.1029/2007JD008609

Dessler, A. E., Ye, H., Wang, T., Schoeberl, M. R., Oman, L. D., Douglass, A. R., et al. (2016). Transport of ice into the stratosphere and the humidification of the stratosphere over the 21st century. *Geophysical Research Letters*, *43*, 2323–2329. https://doi.org/10.1002/2016GL067991

Dinh, T., & Fueglistaler, S. (2014). Microphysical, radiative, and dynamical impacts of thin cirrus clouds on humidity in the tropical tropopause layer and lower stratosphere. *Geophysical Research Letters*, *41*, 6949–6955. https://doi.org/10.1002/2014GL061289

Dinh, T., Podglajen, A., Hertzog, A., Legras, B., & Plougonven, R. (2016). Effect of gravity wave temperature fluctuations on homogeneous ice nucleation in the tropical tropopause layer. *Atmospheric Chemistry and Physics*, *16*(1), 35–46. https://doi.org/10.5194/acp-16-35-2016

Dvortsov, V. L., & Solomon, S. (2001). Response of the stratospheric temperatures and ozone to the past and future increases in stratospheric humidity. *Journal of Geophysical Research*, *106*(D7), 7505–7514. https://doi.org/10.1029/2000JD900637

Folkins, I., & Martin, R. V. (2005). The vertical structure of tropical convection and its impact on the budgets of water vapor and ozone. *Journal of the Atmospheric Sciences*, *62*(5), 1560–1573. https://doi.org/10.1175/JAS3407.1

Forster, P. M. F., & Shine, K. P. (2002). Assessing the climate impact of trends in stratospheric water vapor. *Geophysical Research Letters*, *29*(6), 1086. https://doi.org/10.1029/2001GL013909

Frey, W., Borrmann, S., Fierli, F., Weigel, R., Mitev, V., Matthey, R., et al. (2014). Tropical deep convective life cycle: Cb-anvil cloud microphysics from high-altitude aircraft observations. *Atmospheric Chemistry and Physics*, *14*(23), 13,223–13,240. https://doi.org/10.5194/acp-14-13223-2014

Frey, W., Borrmann, S., Kunkel, D., Weigel, R., de Reus, M., Schlager, H., et al. (2011). In situ measurements of tropical cloud properties in the West African Monsoon: Upper tropospheric ice clouds, mesoscale convective system outflow, and subvisual cirrus. *Atmospheric Chemistry and Physics*, *11*(12), 5569–5590. https://doi.org/10.5194/acp-11-5569-2011

Frey, W., Schofield, R., Hoor, P., Kunkel, D., Ravegnani, F., Ulanovsky, A., et al. (2015). The impact of overshooting deep convection on local transport and mixing in the tropical upper troposphere/lower stratosphere (UTLS). *Atmospheric Chemistry and Physics*, *15*(11), 6467–6486. https://doi.org/10.5194/acp-15-6467-2015

Fueglistaler, S., & Baker, M. B. (2006). A modeling study of the impact of cirrus clouds on the moisture budget of the upper troposphere. *Atmospheric Chemistry and Physics*, *6*(5), 1425–1434. https://doi.org/10.5194/acp-6-1425-2006

Fueglistaler, S., Dessler, A. E., Dunkerton, T. J., Folkins, I., Fu, Q., & Mote, P. W. (2009). Tropical tropopause layer. *Reviews of Geophysics*, *47*, RG1004. https://doi.org/10.1029/2008RG00267

Gill, A. E. (1980). Some simple solutions for heat-induced tropical circulation. *Quarterly Journal of the Royal Meteorological Society*, *106*(449), 447–462. https://doi.org/10.1002/qj.49710644905

Grosvenor, D. P., Choularton, T. W., Coe, H., & Held, G. (2007). A study of the effect of overshooting deep convection on the water content of the TTL and lower stratosphere from cloud resolving model simulations. *Atmospheric Chemistry and Physics*, *7*(18), 4977–5002. https://doi.org/10.5194/acp-7-4977-2007

Heymfield, A. J., & Westbrook, C. D. (2010). Advances in the estimation of ice particle fall speeds using laboratory and field measurements. *Journal of the Atmospheric Sciences*, *67*(8), 2469–2482. https://doi.org/10.1175/2010JAS3379.1

Jensen, E. J., Ackerman, A. S., & Smith, J. A. (2007). Can overshooting convection dehydrate the tropical tropopause layer? *Journal of Geophysical Research*, *112*, D11209. https://doi.org/10.1029/2006JD007943

Jensen, E. J., Lawson, P., Baker, B., Pilson, B., Mo, Q., Heymsfield, A. J., et al. (2009). On the importance of small ice crystals in tropical anvil cirrus. *Atmospheric Chemistry and Physics*, *9*(15), 5519–5537. https://doi.org/10.5194/acp-9-5519-2009

Jensen, E. J., Lawson, R. P., Bergman, J. W., Pfister, L., Bui, T. P., & Schmitt, C. G. (2013). Physical processes controlling ice concentrations in synoptically forced, midlatitude cirrus. *Journal of Geophysical Research: Atmospheres*, *118*, 5348–5360. https://doi.org/10.1002/jgrd.50421

Jensen, E. J., & Pfister, L. (2004). Transport and freeze-drying in the tropical tropopause layer. *Journal of Geophysical Research*, *109*, D02207. https://doi.org/10.1029/2003JD004022

Jensen, E. J., Pfister, L., Bui, T., Weinheimer, A., Weinstock, E., Smith, J., et al. (2005). Formation of a tropopause cirrus layer observed over Florida during CRYSTAL-FACE. *Journal of Geophysical Research*, *110*, L01808. https://doi.org/10.1029/2004JD004671

Jensen, E. J., Pfister, L., & Bui, T. P. (2012). Physical processes controlling ice concentrations in cold cirrus near the tropical tropopause. *Journal of Geophysical Research*, *117*, D11205. https://doi.org/10.1029/2011JD017319

Jensen, E. J., Pfister, L., Bui, T.-P., Lawson, P., & Baumgardner, D. (2010). Ice nucleation and cloud microphysical properties in tropical tropopause cirrus. *Atmospheric Chemistry and Physics*, *10*(3), 1369–1384. https://doi.org/10.5194/acp-10-1369-2010

Jensen, E. J., Thornberry, T. D., Rollins, A. W., Ueyama, R., Pfister, L., Bui, T., et al. (2017). Physical processes controlling the spatial distributions of relative humidity in the tropical tropopause layer over the Pacific. *Journal of Geophysical Research: Atmospheres*, *122*, 6094–6107. https://doi.org/10.1002/2017JD026632

Johnson, D. G., Jucks, K. W., Traub, W. A., & Chance, K. V. (2001). Isotopic composition of stratospheric water vapor: Implications for transport. *Journal of Geophysical Research*, *106*(D11), 12,219–12,226. https://doi.org/10.1029/2000JD900764

Keith, D. W. (2000). Stratosphere-troposphere exchange: Inferences from the isotopic composition of water vapor. *Journal of Geophysical Research*, *105*(D12), 15,167–15,173. https://doi.org/10.1029/2000JD900130

Kim, J., Randel, W. J., & Birner, T. (2018). Convectively driven tropopause-level cooling and its influences on stratospheric moisture. *Journal of Geophysical Research: Atmospheres*, *123*, 590–606. https://doi.org/10.1002/2017JD027080

Kim, J.-E., & Alexander, M. J. (2013). A new wave scheme for trajectory simulations of stratospheric water vapor. *Geophysical Research Letters*, *40*, 5286–5290. https://doi.org/10.1002/grl.50963

Koop, T., Luo, B., Tsias, A., & Peter, T. (2000). Water activity as the determinant for homogeneous ice nucleation in aqueous solutions. *Nature*, *406*(6796), 611–614. https://doi.org/10.1038/35020537

Krämer, M., Rolf, C., Spelten, N., Afchine, A., Fahey, D., Jensen, E., et al. (2020). A microphysics guide to cirrus—Part II: Climatologies of clouds and humidity from observations. *Atmospheric Chemistry and Physics*. https://doi.org/10.5194/acp-2020-40

Kritz, M. A., Rosner, S. W., Kelly, K. K., Loewenstein, M., & Chan, K. R. (1993). Radon measurements in the lower tropical stratosphere: Evidence for rapid vertical transport and dehydration of tropospheric air. *Journal of Geophysical Research*, *98*(D5), 8725–8736. https://doi.org/10.1029/92JD02524

Kuang, Z., & Bretherton, C. S. (2004). Convective influence on the heat balance of the tropical tropopause layer: A cloud-resolving model study. *Journal of the Atmospheric Sciences*, *61*(23), 2919–2927. https://doi.org/10.1175/JAS-3306.1

Lawson, R. P., Pilson, B., Baker, B., Mo, Q., Jensen, E., Pfister, L., & Bui, P. (2008). Aircraft measurements of microphysical properties of subvisible cirrus in the tropical tropopause layer. *Atmospheric Chemistry and Physics*, *8*(6), 1609–1620. https://doi.org/10.5194/acp-8-1609-2008

Lawson, R. P., Woods, S., Jensen, E., Erfani, E., Gurganus, C., Gallagher, M., et al. (2019). A review of ice particle shapes in cirrus formed in situ and in anvils. *Journal of Geophysical Research: Atmospheres*, *124*, 10,049–10,090. https://doi.org/10.1029/2018JD030122

Liu, Y. S., Fueglistaler, S., & Haynes, P. H. (2010). Advection-condensation paradigm for stratospheric water vapor. *Journal of Geophysical Research*, *115*, D24307. https://doi.org/10.1029/2010JD014352

Livesey, N. J., Read, W. G., Froidevaux, L., Lambert, A., Manney, G. L., Pumphrey, H. C., et al. (2015). Earth Observing System (EOS) Aura Microwave Limb Sounder (MLS): Version 4.2x level 2 data quality and description document, Tech. Rep. JPL D-33509 Rev. A, Jet Propulsion Laboratory, available electronically from https://mls.jpl.nasa.gov/data/v4-2_data_quality_document.pdf

Mace, G. G., Deng, M., Soden, B., & Zipser, E. (2006). Association of tropical cirrus in the 10-15-km layer with deep convective sources: An observational study combining millimeter radar data and satellite-derived trajectories. *Journal of the Atmospheric Sciences*, *63*(2), 480–503. https://doi.org/10.1175/JAS3627.1

Matsuno, T. (1966). Quasi-geostrophic motions in the equatorial area. *Journal of the Meteorological Society of Japan*, *44*(1), 25–43. https://doi.org/10.2151/jmsj1965.44.1_25

Minnis, P., Yost, C. R., Sun-Mack, S., & Chen, Y. (2008). Estimating the top altitude of optically thick ice clouds from thermal infrared satellite observations using CALIPSO data. *Geophysical Research Letters*, *35*, L12801. https://doi.org/10.1029/2008GL033847

Mote, P. W., Rosenlof, K. H., McIntyre, M. E., Carr, E. S., Gille, J. C., Holton, J. R., et al. (1996). An atmospheric tape-recorder: The imprint of tropical tropopause temperatures on stratospheric water vapor. *Journal of Geophysical Research*, *101*(D2), 3989–4006. https://doi.org/10.1029/95JD03422

Moyer, E. J., Irion, F. W., Yung, L., & Gunson, M. R. (1996). ATMOS stratospheric deuterated water and implications for troposphere-stratosphere transport. *Geophysical Research Letters*, *23*(17), 2385–2388. https://doi.org/10.1029/96GL01489

Nielsen, J. K., Larsen, N., Cairo, F., Di Donfrancesco, G., Rosen, J. M., Durry, G., et al. (2007). Solid particles in the tropical lowest stratosphere. *Atmospheric Chemistry and Physics*, *7*(3), 685–695. https://doi.org/10.5194/acp-7-685-2007

Pfister, L., Selkirk, H. B., Jensen, E. J., Schoeberl, M. R., Toon, O. B., Browell, E. V., et al. (2001). Aircraft observations of thin cirrus clouds near the tropical tropopause. *Journal of Geophysical Research*, *106*(D9), 9765–9786. https://doi.org/10.1029/2000JD900648

Randel, W. J., & Jensen, E. J. (2013). Physical processes in the tropical tropopause layer and their roles in a changing climate. *Nature Geoscience*, *6*(3), 169–176. https://doi.org/10.1038/ngeo1733

Randel, W. J., Moyer, E., Park, M., Jensen, E., Bernath, P., Walker, K., & Boone, C. (2012). Global variations of HDO and HDO/H_2O ratios in the upper troposphere and lower stratosphere derived from ACE-FTS satellite measurements. *Journal of Geophysical Research*, *117*, D06303. https://doi.org/10.1029/2011JD016632

Randel, W. J., & Park, M. (2019). Diagnosing observed stratospheric water vapor relationships to the cold point tropical tropopause. *Journal of Geophysical Research: Atmospheres*, *124*, 7018–7033. https://doi.org/10.1029/2019JD030648

Randel, W. J., & Wu, F. (2005). Kelvin wave variability near the equatorial tropopause observed in GPS radio occultation measurements. *Journal of Geophysical Research*, *110*, D03102. https://doi.org/10.1029/2004JD005006

Randel, W. J., Wu, F., Oltmans, S. J., Rosenlof, K., & Nedoluha, G. E. (2004). Interannual changes of stratospheric water vapor and correlations with tropical tropopause temperatures. *Journal of the Atmospheric Sciences*, *61*(17), 2133–2148. https://doi.org/10.1175/1520-0469(2004)061<2133:ICOSWV>2.0.CO;2

Read, W. G., Lambert, A., Bacmeister, J., Cofield, R. E., Christensen, L. E., Cuddy, D. T., et al. (2007). Aura Microwave Limb Sounder upper tropospheric and lower stratospheric H_2O and relative humidity with respect to ice validation. *Journal of Geophysical Research*, *112*, D24S35. https://doi.org/10.1029/2007JD008752

Riese, M., Ploeger, F., Rap, A., Vogel, B., Konopka, P., Dameris, M., & Forster, P. (2012). Impact of uncertainties in atmospheric mixing on simulated UTLS composition and related radiative effects. *Journal of Geophysical Research*, *117*, D16305. https://doi.org/10.1029/2012JD017751

Robinson, F. J., & Sherwood, S. C. (2006). Modeling the impact of convective entrainment on the tropical tropopause. *Journal of the Atmospheric Sciences*, *63*(3), 1013–1027. https://doi.org/10.1175/JAS3673.1

Schiller, C., Grooβ, J.-U., Konopka, P., Plöger, F., Silva dos Santos, F. H., & Spelten, N. (2009). Hydration and dehydration at the tropical tropopause. *Atmospheric Chemistry and Physics*, *9*(24), 9647–9660. https://doi.org/10.5194/acp-9-9647-2009

Schoeberl, M. R., Dessler, A., Wang, T., Avery, M., & Jensen, E. J. (2014). Cloud formation, convection, and stratospheric dehydration. *Earth and Space Science*, *1*, 1–17. https://doi.org/10.1002/2014EA000014

Schoeberl, M. R., Dessler, A., Ye, H., Wang, T., Avery, M., & Jensen, E. J. (2016). The impact of gravity waves and cloud nucleation threshold on stratospheric water and tropical tropospheric cloud fraction. *Earth and Space Science*, *3*, 295–305. https://doi.org/10.1002/2016EA000180

Schoeberl, M. R., & Dessler, A. E. (2011). Dehydration of the stratosphere. *Atmospheric Chemistry and Physics*, *11*(16), 8433–8446. https://doi.org/10.5194/acp-11-8433-2011

Schoeberl, M. R., Jensen, E., Podglajen, A., Coy, L., Lodha, C., Candido, S., & Carver, R. (2017). Gravity wave spectra in the lower stratosphere diagnosed from project loon balloon trajectories. *Journal of Geophysical Research: Atmospheres*, *122*, 8517–8524. https://doi.org/10.1002/2017JD026471

Schoeberl, M. R., Jensen, E. J., Pfister, L., Ueyama, R., Avery, M., & Dessler, A. E. (2018). Convective hydration of the upper troposphere and lower stratosphere. *Journal of Geophysical Research: Atmospheres*, *123*, 4583–4593. https://doi.org/10.1029/2018JD028286

Schoeberl, M. R., Jensen, E. J., Pfister, L., Ueyama, R., Wang, T., Selkirk, H., et al. (2019). Water vapor, clouds, and saturation in the tropical tropopause layer. *Journal of Geophysical Research: Atmospheres*, *124*, 3984–4003. https://doi.org/10.1029/2018JD029849

Schoeberl, M. R., Jensen, E. J., & Woods, S. (2015). Gravity waves amplify upper tropospheric dehydration by clouds. *Earth and Space Science*, *2*, 485–500. https://doi.org/10.1002/2015EA000127

Selkirk, H. B. (1993). The tropopause cold trap in the Australian monsoon during STEP/AMEX 1987. *Journal of Geophysical Research*, *98*(D5), 8591–8610. https://doi.org/10.1029/92JD02932

Sherwood, S. C., Chae, J.-H., Minnis, P., & McGill, M. (2004). Underestimation of deep convective cloud tops by thermal imagery. *Geophysical Research Letters*, *31*, L11102. https://doi.org/10.1029/2004GL019699

Sherwood, S. C., & Dessler, A. E. (2001). A model for transport across the tropical tropopause. *Journal of the Atmospheric Sciences*, *58*, 765–779. https://doi.org/10.1175/520-0469(2001)058<0765:AMFTAT>2.0.CO;2

Sherwood, S. C., Horinouchi, T., & Zelenzik, H. A. (2003). Convective impact on temperatures observed near the tropical tropopause. *Journal of the Atmospheric Sciences*, *60*(15), 1847–1856. https://doi.org/10.1175/1520-0469(2003)060<1847:CIOTON>2.0.CO;2

Smith, J. B., Wilmouth, D. M., Bedka, K. M., Bowman, K. P., Homeyer, C. R., Dykema, J. A., et al. (2017). A case study of convectively sourced water vapor observed in the overworld stratosphere over the United States. *Journal of Geophysical Research: Atmospheres*, *122*, 9529–9554. https://doi.org/10.1002/2017JD026831

Sölch, I., & Kärcher, B. (2010). A large-eddy model for cirrus clouds with explicit aerosol and ice microphysics and Lagrangian ice particle tracking. *Quarterly Journal of the Royal Meteorological Society*, *136*(653), 2074–2093. https://doi.org/10.1002/qj.689

Solomon, S., Rosenlof, K., Portmann, R., Daniel, J., Davis, S., Sanford, T., & Plattner, G.-K. (2010). Contributions of stratospheric water vapor changes to decadal variations in the rate of global warming. *Science*, *327*(5970), 1219–1223. https://doi.org/10.1126/science.1182488

Stenke, A., & Grewe, V. (2005). Simulation of stratospheric water vapor trends: Impact on stratospheric ozone chemistry. *Atmospheric Chemistry and Physics*, *5*(5), 1257–1272. https://doi.org/10.5194/acp-5-1257-2005

Ueyama, R., Jensen, E. J., & Pfister, L. (2018). Convective influence on the humidity and clouds in the tropical tropopause layer during boreal summer. *Journal of Geophysical Research: Atmospheres*, *123*, 7576–7593. https://doi.org/10.1029/2018JD028674

Ueyama, R., Jensen, E. J., Pfister, L., Diskin, G. S., Bui, T. P., & Dean-Day, J. M. (2014). Dehydration in the tropical tropopause layer: A case study for model evaluation using aircraft observations. *Journal of Geophysical Research: Atmospheres*, *119*, 5299–5316. https://doi.org/10.1002/2013JD021381

Ueyama, R., Jensen, E. J., Pfister, L., & Kim, J.-E. (2015). Dynamical, convective, and microphysical control on wintertime distributions of water vapor and clouds in the tropical tropopause layer. *Journal of Geophysical Research: Atmospheres*, *120*, 10,483–10,500. https://doi.org/10.1002/2015JD023318

Vogel, B., Feck, T., & Grooß, J.-U. (2011). Impact of stratospheric water vapor enhancements caused by CH_4 and H_2O increase on polar ozone loss. *Journal of Geophysical Research*, *116*, D05301. https://doi.org/10.1029/2010JD014234

Wang, X., Dessler, A. E., Schoeberl, M. R., Yu, W., & Wang, T. (2019). Impact of convectively lofted ice on the seasonal cycle of water vapor in the tropical tropopause layer. *Atmospheric Chemistry and Physics*, *19*(23), 14,621–14,636. https://doi.org/10.5194/acp-19-14621-2019

Yang, Q., Fu, Q., & Hu, Y. (2010). Radiative impacts of clouds in the tropical tropopause layer. *Journal of Geophysical Research*, *115*, D00H12. https://doi.org/10.1029/2009JD012393

Ye, H., Dessler, A. E., & Yu, W. (2018). Effects of convective ice evaporation on interannual variability of tropical tropopause layer water vapor. *Atmospheric Chemistry and Physics*, *18*(7), 4425–4437. https://doi.org/10.5194/acp-18-4425-2018

Zipser, E. J., Cecil, D. J., Liu, C., Nesbitt, S. W., & Yorty, D. P. (2006). Where are the most intense thunderstorms on Earth? *Bulletin of the American Meteorological Society*, *87*(8), 1057–1072. https://doi.org/10.1175/BAMS-87-8-1057